AFM studies of surface morphologies of sputtered SrTiO₃ films and annealed MgO substrates

Q. Meng, R. Moerman, A.H. Sonnenberg, G.J. Gerritsma

Low Temperature Division, Department of Applied Physics, University of Twente, P.O. Box 217, 7500 AE, Enschede, The Netherlands
(Fax: +31-53/489-1099, E-mail: mng@el.utwente.nl; gma@tn.utwente.nl)

Abstract. Atomic force microscopy (AFM) is applied to study the surface morphologies and growth mechanisms of sputtered SrTiO₃ films on single-crystal MgO(100) substrates. Meanwhile, surface morphologies of as-polished and post-annealed MgO(100) substrates are investigated as well. Effects of the miscut (or misorientation) of the substrate surface on morphologies and growth mechanisms are discussed. For comparison, a typical surface morphology and growth mechanism of the spiral island structure in sputtered $PrBa_2Cu_3O_{7-\delta}$ films on MgO(100) substrates are presented.

PACS: 68.55; 77.55; 81.40

The single-crystal MgO substrate is one of the promising substrates to be used for HTS (high T_c superconducting) applications in the field of high-frequency devices as MgO has a relatively low dielectric loss at the high frequency compared with SrTiO₃ substrates and has a dielectric constant close to that of Al_2O_3 substrate, which is quite often used in the microwave community [1–4]. A multilayer technique has been developed to fabricate HTS ramp-type Josephson junctions (RTJJs) on SrTiO₃(100) substrates by using $DyBa_2Cu_3O_{7-\delta}$ (DBCO) as superconducting electrodes and $PrBa_2Cu_3O_{7-\delta}$ (PBCO) as a barrier material [5, 6]. RTJJs were developed in order to use the longer coherence length in the a-b plane of c-axis-oriented HTS layers through the ramp. Briefly speaking, the patterned ramps are created by Ar ion-beam etching under a certain angle (e.g. 45°) with respect to the substrate surface after deposition of DBCO and PBCO layers. Then PBCO and DBCO layers are deposited subsequently on these etched ramps to form RTJJs [5]. There are some problems in preparing RTJJs using DBCO and PBCO layers on MgO(100) substrates. One of the problems is that transformation twins and grain boundaries may be formed in DBCO and PBCO films because of a large lattice mismatch ($\approx 8.8\%$) between the a-b plane of DBCO (or PBCO) film and the (100) plane of MgO substrate. These defects have been observed in $YBa_2Cu_3O_{7-\delta}$ (YBCO) films when they are deposited on MgO(100) substrates [7, 8]. Especially, grain boundaries may be formed in the PBCO barrier layer at the corner between the etched ramp

and flat surface of MgO substrate and at interface edges between MgO surface and DBCO layer on the ramp surface because the c axis of the PBCO layer grows preferably along the normal of the etched ramp surface but PBCO can grow epitaxially on the DBCO layer. Such grain boundaries have been observed in YBCO films when they are deposited on the ramp of MgO(100) substrates [9–12]. This in turn leads to grain boundaries in the subsequently deposited DBCO electrode layer and results in undesired weak-link effects in prepared RTJJs [13].

In order to eliminate the formation of the grain boundaries in DBCO and PBCO layers, we decided to use a SrTiO₃ (STO) thin film as a buffer layer on MgO(100) substrates and to prepare RTJJs on the ramp of the STO buffer layer rather than directly on MgO substrate. It has been reported that a STO thin film is suitable to prepare RTJJs on SOS (silicon on sapphire) substrates when it is used in a complex multilayer buffer system [13]. Besides the ability to use a STO buffer layer to fabricate RTJJs avoiding additional grain-boundary weak links, one of the undesired effects that must be considered is that the dielectric constant of a STO film could be as high as a STO crystal substrate. However, due to the small thickness (e.g. 30–40 nm), a STO buffer layer hardly affects the dielectric properties of MgO substrates [2, 3, 13].

Various attempts have been made to obtain a suitable STO buffer layer on MgO(100) substrates in order to improve the quality of the subsequent deposition of YBCO-type superconducting thin films [1, 2, 14, 15]. The improvement of the crystallinity and superconducting properties of YBCO films on STO-buffered MgO(100) substrates has been achieved [1, 2]. However, all those studies were carried out using pulsed laser deposition (PLD). To our knowledge, there has been no report on sputtered STO films on MgO substrates and no report on the fabrication of RTJJs on STO-buffered MgO substrates yet. In our case, RTJJs using the multilayer technique are mainly fabricated using a sputter system [6]. Therefore, an attempt to obtain suitable STO buffer layers on MgO substrates by sputtering was carried out. By optimizing sputtering conditions, smooth and epitaxial STO films on MgO(100) substrates have been achieved [16]. Consequently, RTJJs fabricated on STO-buffered MgO(100) substrates have shown superconducting

and tunneling properties comparable to those on STO substrates [17].

In this paper, we present studies on surface morphologies and growth mechanisms of sputtered STO films by using AFM. Meanwhile, the morphology of as-polished and post-annealed MgO substrates are also studied in order to obtain a high-quality substrate surface for the smooth and epitaxial film growth, taking especial care about the in-plane epitaxial formation. The effects of miscut (or misorientation) of the MgO substrate surface on morphology and growth mechanism are discussed. A miscut of about 1° between the (001) plane and substrate surface is expected for our used MgO substrates according to our XRD (X-ray diffraction) measurements [16]. For comparison, a typical surface morphology and growth mechanism of the spiral island structure in sputtered PBCO films on MgO(100) substrates are presented.

1 Experimental

STO films were deposited on single-crystal MgO(100) substrates by off-axis rf magnetron sputtering from a $SrTiO_3$ target [6]. The optimal sputtering conditions are as follows. The deposition temperature was 770 °C and the sputtering pressure was 0.25 mbar using an Ar/O_2 (50:50) gas mixture. The substrate was positioned in the vicinity of the visible plasma close to the target. The rf power was 90 W. The deposition rate was about 37 nm/h.

Special care was taken in handling the polished surface of the MgO substrate because of its hygroscopic nature [1, 2]. However, it was found that water and other contaminants on the polished MgO surface can be significantly removed by baking for a while, e.g. 10–30 min in the vacuum chamber around the deposition temperature, e.g. 770 °C–790 °C. Therefore, in our case, MgO(100) substrates were cleaned ultrasonically in acetone and ethanol without any other special treatment and then blown dry with N_2. The substrate ($10 \times 5 \times 0.5$ mm) was glued onto a heater block using silver paint and heated up to the deposition temperature in the sputter chamber for about 30 min while the chamber was pumped down to a pressure about 10^{-6} mbar. After deposition, the film was left to cool down to 120 °C in situ with flowing O_2 at a pressure of 200 mbar.

On the other hand, in order to reduce the damage on the substrate surface caused by mechanical polishing and to reconstruct the surface to achieve atomically flat steps, annealing of MgO substrates at temperatures between 1000 °C and 1100 °C was carried out in a furnace using a quartz-tube holder and a little O_2 flow according to reports in [18–22].

AFM measurements were performed under an ambient atmosphere at room temperature using a commercial setup of Nanoscope III, The Si_3N_4 tips were applied using the contact mode. The reliability and reproducibility of the recorded images were carefully established.

2 Results and discussion

2.1 Surface morphologies of ultrasonically cleaned and baked MgO substrates

First of all, the polished surface of a MgO(100) substrate was examined by using AFM. Figure 1 shows a surface image of
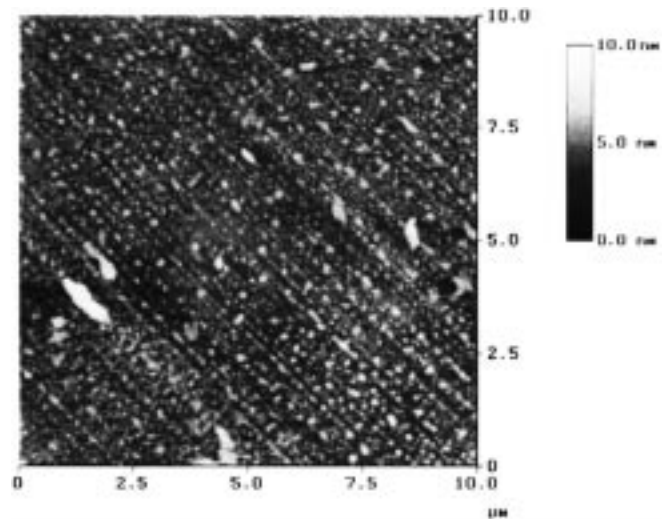

Fig. 1. An AFM image of the polished surface of a MgO(100) substrate which was cleaned ultrasonically in acetone and ethanol (Substrate A)

a substrate (Substrate A) that was ultrasonically rinsed before it was measured. The residual contamination is clearly displayed in a shape of irregular hills with a submicron size along the scratches [19, 20]. The height of the hills is about 10 nm as indicated by a height scale shown at the right-hand side of the image. The contamination possibly originates from the mechanical polishing and the reaction with the ambient air and water. The reaction with air and water may lead to hydroxides and carbonates on the surface, which has been determined by XPS (X-ray photoelectron spectroscopy) measurements and has also been reported in [20]. Such a surface contamination is bad for thin film deposition.

However, in our case, the substrates are always heated up to a high deposition temperature in the vacuum. Therefore, it is important to examine the quality of the substrate surface after being heated. Figure 2 gives the surface image of a MgO substrate (Substrate B) that was heated up to
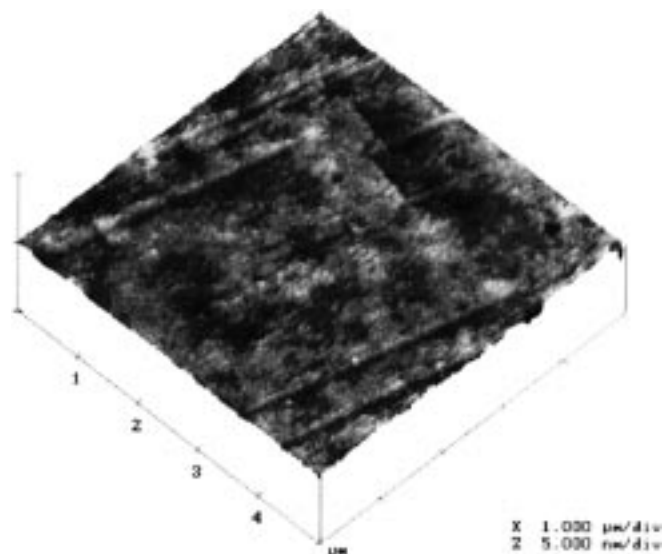

Fig. 2. An AFM image of the baked surface of a MgO(100) substrate which was heated in the vacuum chamber at 790 °C for 10 min (Substrate B)

790 °C in the sputter chamber for 10 min. Since no annealing effect could be expected when MgO substrates are heated at 790 °C (which is much lower than the effective annealing temperature of MgO substrate, e.g. 1000 °C), the substrate was just baked. Therefore, such a heated substrate is termed a *baked substrate* in this paper in order to distinguish from an annealed substrate. The image in Fig. 2 demonstrates that the surface was significantly cleaned after being baked besides ultrasonic rinsing. The scratches due to the mechanical polishing are clearly observed, as shown in a shape of linear pits which are about 0.5 nm in depth. Compared with the ultrasonically cleaned surface, the baked surface is more suitable for the thin film deposition, which is confirmed by the following results.
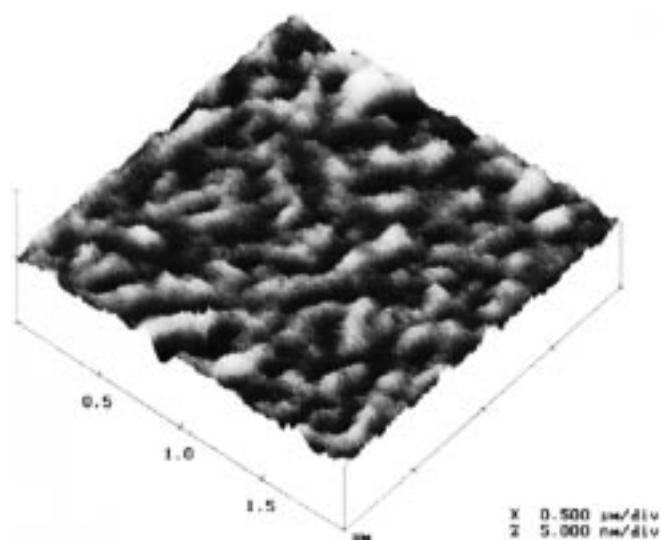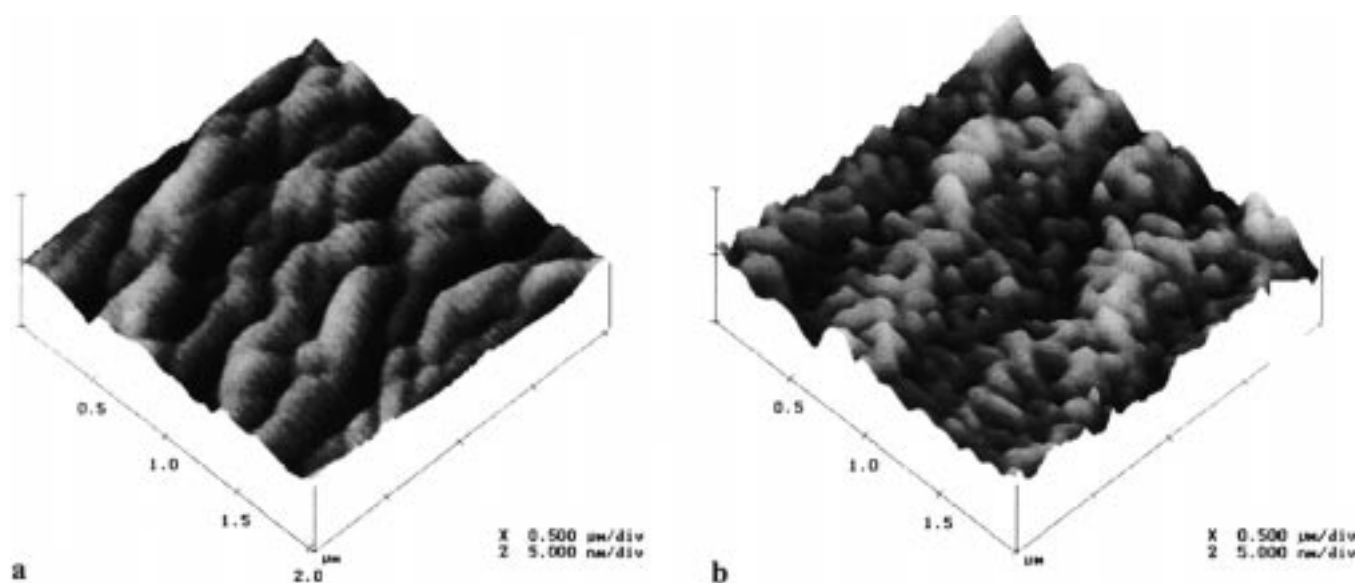

Fig. 3. An AFM image of a deposited SrTiO$_3$ film (Film A, about 37 nm in thickness) on a baked MgO(100) substrate

2.2 Surface morphologies of SrTiO$_3$ films on the baked and annealed MgO substrates

Figure 3 shows the surface image of a STO film (Film A, about 37 nm in thickness) that was deposited on a baked MgO substrate. The image indicates a very smooth surface with a granular topography (the measured rms roughness $\sigma < 1$ nm) although the film surface is rougher than the baked substrate surface. Such a smooth surface is very suitable for the subsequent deposition of the smooth DBCO and PBCO layers. This has been demonstrated in our work [16]. The main results are summarized as follows. The STO film in Fig. 3 has shown a good crystallinity with a single [001] orientation perpendicular to the film surface as measured by XRD. The DBCO on such a STO-buffered MgO substrate has shown a single [001] orientation perpendicular to the film surface and good superconducting properties (i.e. superconducting transition temperature of $T_c = 89$ K ($R = 0$) and resistance ratio of $R(300\,\text{K})/R(100\,\text{K}) \approx 3$). The (001) lattice planes of the STO buffer layer and DBCO film are clearly observed in a cross-sectional TEM (transmission electron microscopy) micrograph. They are parallel to the MgO substrate surface.

However, STO films deposited on annealed MgO substrates are not so encouraging. Figures 4 and 5 give the surface images of two annealed MgO(100) substrates and STO films deposited on them, respectively. The substrate in Fig. 4a (Substrate C) was annealed at 1000 °C for 12 h (excluding the time of heating up and cooling down). The substrate in Fig. 5a (Substrate D) was annealed at 1050 °C for 10 h. Compared with the baked substrate surface shown in Fig. 2, the crystallinity of the annealed surface seems better but the surface roughness increases as reported in [21, 22]. A remarkable result is that Substrate D exhibits the atomically terraced steps as reported in annealed STO substrates [20] and annealed MgO substrates [22]. The height of the steps is about one or two unit cells (0.42–0.84 nm) and the width of flat terraces is about 0.5 μm. Consequently, the surface mor-

Fig. 4a,b. AFM images of an annealed MgO(100) substrate (Substrate C) (**a**) and a deposited SrTiO$_3$ film (Film B, about 37 nm in thickness) on this annealed substrate (**b**). The substrate was annealed at 1000 °C for 12 h
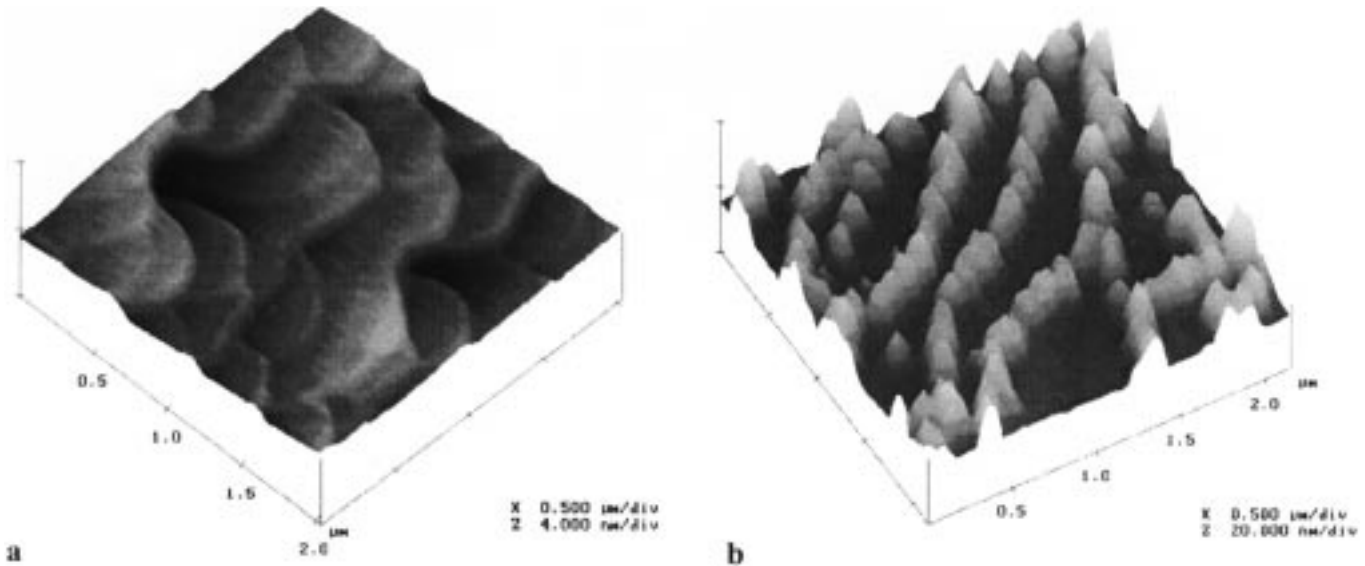
Fig. 5a,b. AFM images of an annealed MgO(100) substrate (Substrate D) (**a**) and a deposited $SrTiO_3$ film (Film C, about 74 nm in thickness) on this annealed substrate (**b**). The substrate was annealed at 1050 °C for 10 h

phologies of deposited STO films on these two substrates are completely different although their deposition conditions and the film thickness are the same, i.e. about 37 nm by one-hour deposition. In Fig. 4b, the film (Film B) on Substrate C shows a similar granular topography to Film A on the baked substrate (see Fig. 3). However, the surface roughness of Film B is increased. XRD measurements indicated that Film B also has a good crystallinity with a single [001] orientation perpendicular to the film surface. This suggests that Film B could also be good for the subsequent deposition of smooth DBCO and PBCO films.

Furthermore, row-like appearances are clearly displayed in two images shown in Fig. 4. Comparing the images between the substrate and the film, it is worth noting that the film was growing along the "rows" of the annealed substrate. Such a film growth mode is remarkably enhanced in the film (Film C) deposited on Substrate D as shown in Fig. 5. The surface image of Film C shows that the nucleation of deposits was along the step edges of the annealed substrate surface, which results in a hill-like morphology as shown in Fig. 5b in which the height of the "hills" is about 20 nm. Such a film with those high hills is undesirable for the subsequent deposition. Therefore, an annealed substrate surface is not suitable for thin film deposition if the steps are too high, e.g. higher than one unit cell (> 0.4 nm) because hills (i.e. particles) could be formed along the step edges. However, the formation of such big particles also depends on the deposition conditions. The nucleation of deposits along the step edges of the substrate surface has been studied in DBCO films deposited on STO substrates [23]. Optimization for film depositing and substrate annealing is required to obtain smooth and epitaxial STO films.

In order to clarify the quality of the annealed MgO substrates, a systematic study was carried out under different annealing temperatures from 1000 °C to 1100 °C and different annealing times from 6 to 14 h. Some problems were found concerning the reproducibility of the annealed surface. One is attributed to the miscut (or misorientation) of the polished substrate surface [20]. Another big problem is the segregation

of Ca on the MgO(100) substrate surface. The segregation of Ca results in large particles on the substrate surface, which are about 0.1–0.5 μm in size and 30–50 nm in height with number of 1–5 per μm^2 as measured by AFM. Variation of the Ca segregation depends on the impurity of MgO substrates and annealing conditions, which have been studied by several groups [22, 24–27].

2.3 Nucleation and growth mechanisms of $SrTiO_3$ and $PrBa_2Cu_3O_{7-\delta}$ films on baked MgO substrates

Figure 6 shows AFM images of a STO film (Film D) on a baked MgO(100) substrate. The film was deposited under the same conditions as Films B and C but deposited for 2 h, so that the thickness would be about 74 nm. Figure 6a gives an overview image of the film, which reveals a cross-shape morphology. This could be attributed to the miscut defects formed on the substrate surface as reported in STO substrates [20]. Nevertheless, this image implies that this substrate surface is as flat as that shown in Fig. 2. As a result, the STO film deposited on this substrate exhibits a particular terraced-island structure which is enlarged as shown in the following graphs. In Fig. 6b, the deflection image (on the right-hand side) reveals the clear terraced-steps and islands which are formed particularly along the cross-defect tracks. This suggests that the defects on the substrate surface may contribute to the nucleation sites for the island growth. The details of the terraced-island structure are given in Fig. 6c. A height profile along a line as indicated in the graph is plotted in Fig. 6d. The height and width of the terraces are about 0.2 nm and 22 nm, respectively, as measured by two arrows. It is noteworthy that the measured height is about the distance between TiO and SrO_2 atom-planes in a $SrTiO_3$ crystal. There have been some reports on surface morphology of STO films on MgO and STO substrates [3, 28, 29]. However, we note that this is the first time that such a terraced-island structure is reported in a sputtered $SrTiO_3$ film on MgO substrate. One interesting feature of the presented STO film is its terraced
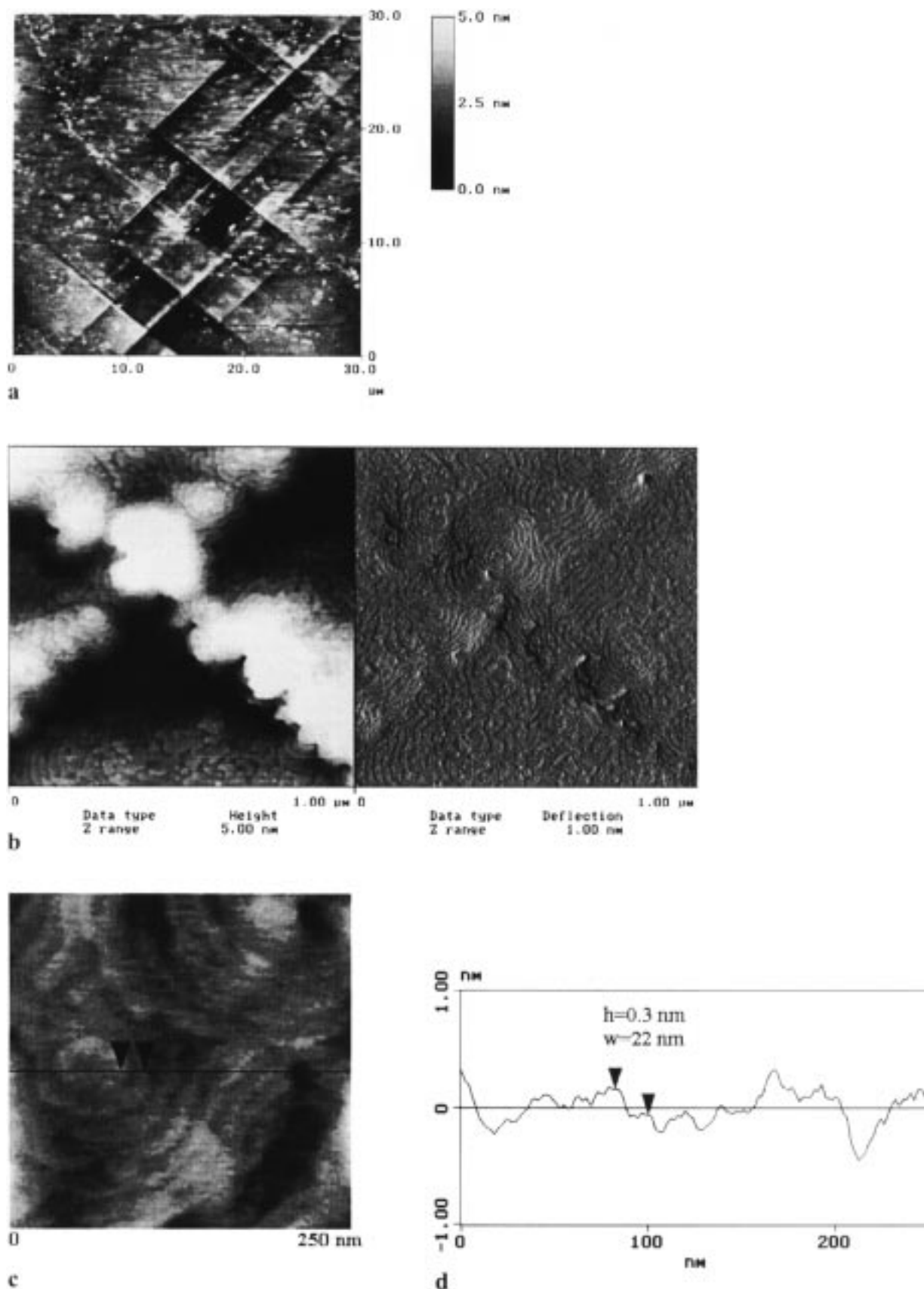
Fig. 6a–d. AFM images of a deposited SrTiO$_3$ film (Film D, about 74 mn in thickness) on a baked MgO(100) substrate. **a** A overview image (30 × 30 μm) showing the cross-shaped defects on the substrate surface. **b** High-resolution height and defection images which were recorded at the same time. **c** A detailed image taken partly from the height image **b**. **d** A height profile on a line indicated in the image **c**, where *h* is the height of the step and *w* the width of the terrace

steps and islands without any indication of a spiral structure. The spiral terraced-island structure has been observed in c-axis-oriented YBCO-type films on MgO and STO substrates and most of them were observed by STM (scanning tunneling microscopy) [30–35].

In our studies, we observed the spiral terraced-island structure in our sputtered PBCO films on MgO(100) substrates by AFM. Figure 7 gives the images of a PBCO film (Film E) on a baked substrate. The film was deposited by sputtering using a Ar/O_2 (50:50) mixture gas and a H_2O vapor (about 0.1% of total sputtering pressure) under a sputtering pressure of 0.15 mbar and at 790 °C [6]. The film thickness is about 40 nm after 30 min deposition. In Fig. 7a, the deflection image (on the right-hand side) demonstrates the spiral islands as shown in a typical pyramidal shape. The details of a pyramidal-shape spiral island are given in Fig. 7b. The height and width of the spiral terrace are about 0.8 nm and 25 nm, respectively, as measured by two arrows in Fig. 7c.

Such a pronounced island structure results in a rougher surface compared with the STO film surface. This implies that PBCO films are not as good as STO films when they are considered for use as a buffer layer for the preparation of RTJJs on MgO substrates. A study on preparation of RTJJs using PBCO buffer layer on MgO substrates has been reported [12].

The growth of the spiral structure has been explained by a growth model considering the screw dislocations and stacking faults, which are formed during the film growing [30–32]. It has been also observed that the density of screw dislocations decreases with increasing misorientation of the substrate surface as well as the film-growing temperature [33]. Another factor that has been considered, especially in the PBCO-type films deposited on MgO(100) substrates, is attributed to the strain release because of a large lattice mismatch between the film and the substrate [34]. However, as observed in our studies, nonspiral terraced-island growth of STO films on MgO(100) substrates suggests that the formation of the
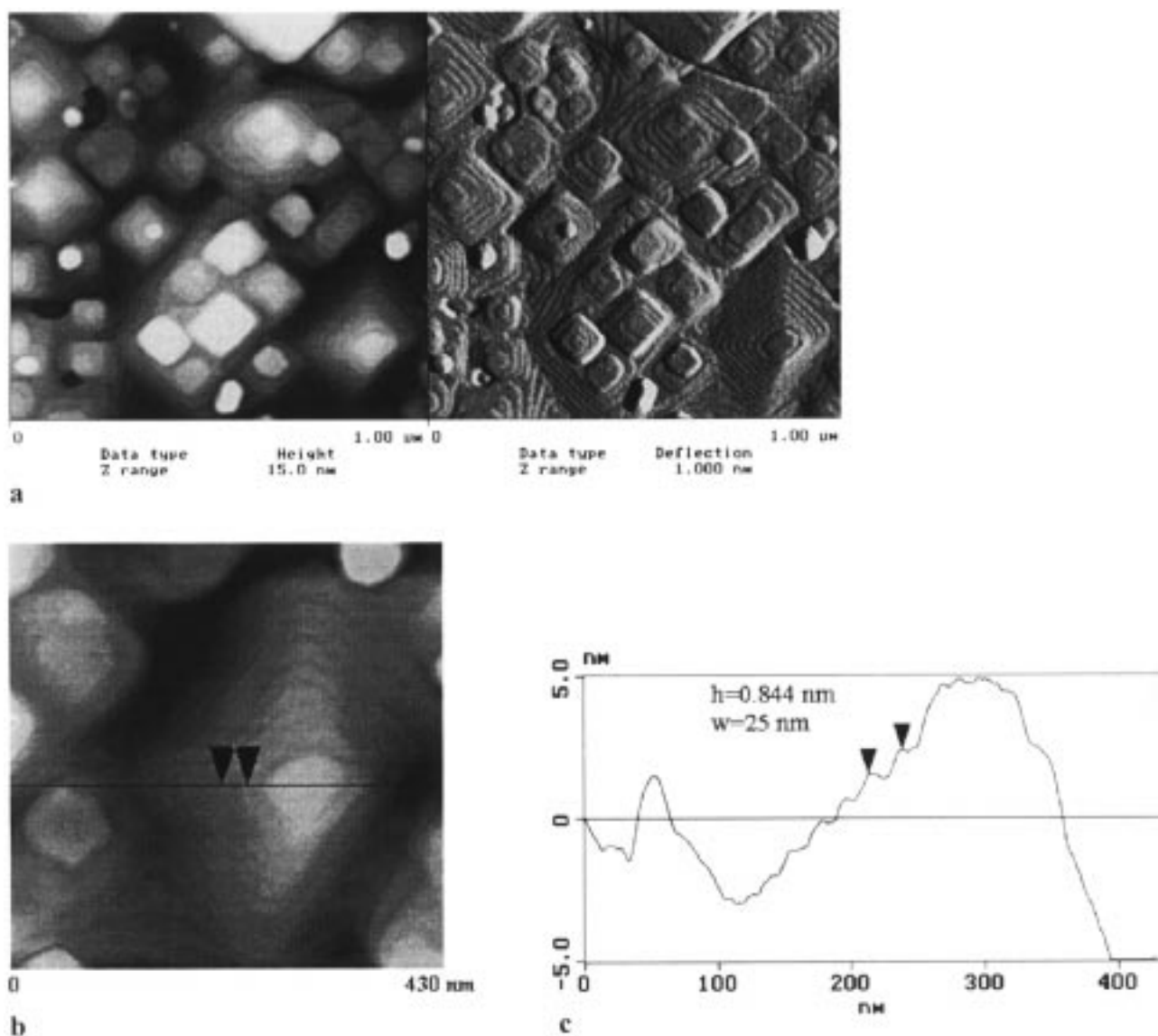
Fig. 7a–c. AFM images of a deposited $PrBa_2Cu_3O_{7-\delta}$ film (Film E, about 40 nm in thickness) on a baked MgO(100) substrate. **a** Height and defection images recorded at the same time. **b** A detailed image taken partly from the height image **a**. **c** A height profile on a line indicated in the image **b**, where h is the height of the step and w the width of the terrace

screw dislocation is an intrinsic property of the YBCO-type films [31]. Moreover, we have also observed spiral terraced-island structures in our sputtered DBCO films on MgO substrates [16].

3 Conclusion

By optimizing sputtering conditions, smooth and epitaxial STO films on MgO(100) substrates have been achieved. Consequently, RTJJs fabricated on STO-buffered MgO(100) substrates have shown superconducting and tunneling properties comparable to those on STO substrates.

The surface morphologies and growth mechanisms of sputtered $SrTiO_3$ and $PrBa_2Cu_3O_{7-\delta}$ films on baked and annealed MgO(100) substrates have been studied by using AFM. Meanwhile, the surface quality of baked and annealed MgO substrates has been examined as well. The STO films on the baked substrates are smoother than those on the annealed substrates because of the smoother surface of the baked substrate. The reconstructed substrate surface with atomically flat terraced-steps has been obtained by annealing the MgO substrate at high temperatures above 1000 °C. However, the films deposited on the stepped substrates showed hills nucleated along the step edges, which is not desirable for use as buffer layer.

The nonspiral terraced-island structure has been observed in a STO film on a baked MgO(100) substrate. In contrast, the spiral terraced-island structure is observed in PBCO and DBCO films on baked MgO(100) substrates. The differences in the surface morphologies and growth mechanisms between the STO and PBCO films is attributed to the different sputtering conditions. However, the miscut or misorientation of the substrate surface could be an important factor on the film growth mechanism and thereby the surface morphology. The effects of the misorientation of the substrate surface are evident when considering the low reproducibility of the annealed substrates.

References

1. J.T. Cheung, I. Gergis, M. James, R.E. DeWaames: Appl. Phys. Lett. **60**, 3180 (1992)
2. V. Boffa, T. Petrisor, L. Ciontea, U. Gambardella, S. Barbanera: Physica C **260**, 111 (1996)
3. M.R. Rao: Appl. Phys. Lett. **69**, 1957 (1996)
4. H. Myoren, M.A.J. Verhoeven, J. Chen, K. Nakajima, T. Yamashita, D.H.A. Blank, H. Rogalla: accepted by IEEE Trans. Appl. Supercond. (1998)
5. J. Gao, W.A.M. Aarnink, G.J. Gerritsma, H. Rogalla: Physica C **171**, 126 (1990); J. Gao, Y. Boguslavskij, B.B.G. Klopman, D. Terpstra, G.J. Gerritsma, H. Rogalla: Appl. Phys. Lett. **59**, 2754 (1991)
6. M.A.J. Verhoeven, A.A. Golubov, G.J. Gerritsma, H. Rogalla: IEEE Trans. Appl. Supercond. **5**, 2095 (1995); M.A.J. Verhoeven, R. Moerman, M.E. Bijlsma, A.J.H.M. Rijnders, D.H.A. Blank, G.J. Gerritsma, H. Rogalla: Appl. Pbys. Lett. **68**, 1276 (1996); M.A.J. Verhoeven: PhD Thesis, University of Twente, Enschede, The Netherlands, ISBN 90-365-08-177 (1996)
7. R. Ramesh, D. Hwang, T.S. Ravi, A. Inam, J.B. Barner, L. Nazar, S.W. Chan, C.Y. Chen, B. Dutta, T. Venkatesan, X.D. Wu: Appl. Phys. Lett. **56**, 2243 (1990)
8. C.B. Eom, J.Z. Sun, B.M. Lairson, S.K. Streiffer, A.F. Marshall, K. Yamamoto, S.M. Anlage, J.C. Bravman, T.H. Geballe: Physica C **171**, 354 (1990)
9. M. Kamei, H. Takahashi, S. Fujino, T. Morishita: Physica C **199**, 425 (1992)
10. S. Tanaka, H. Kado, T. Matsuura, H. Itozaki: IEEE Trans. Appl. Supercond. **3**, 2365 (1993)
11. T. Mitsuzuka, K. Yamaguchi, S. Yoshikawa, K. Hayashi, M. Konishi, Y. Enomoto: Physica C **218**, 229 (1993)
12. P.J. Hirst, M.A. Barnett, N.G. Chew, J.S. Abell, M. Aindow, R.G. Humphreys: Proceedings of EUROCA '97, Veldoven, The Netherlands, July 1997
13. B.D. Hunt, M.C. Foote, W.T. Pike, J.B. Barner, R.P. Vasquez: Physica C **230**, 141 (1994)
14. M. Hiratani, K. Imagawa, K. Takagi: Jpn. J. Appl. Phys. **34**, 254 (1995)
15. R, Kalyanaraman, R.D. Vispute, S. Oktyabrsky, K. Dovidenko, K. Jaganaadham, J. Narayan, J.D. Budai, N. Parikh, A. Suvkhanov: Appl. Phys. Lett. **71**, 1709 (1997)
16. O. Meng. R. Moerman, A.H. Sonnenberg, G.J. Gerritsma: submitted to Physica C
17. H. Myoren: private communication
18. M.G. Norton, S.R. Summertelt, C.B. Carter: Appl. Phys. Lett. **56**, 2246 (1990)
19. S. King, L. Coccia, I.W. Boyd: Appl. Surf. Sci. **86**, 134 (1995)
20. R. Sum, H.P. Lang, H.-J. Güntherodt: Physica C **242**, 174 (1995)
21. N. Ikemiya, A. Kitamura, S. Hara: J. Cryst. Growth **160**, 104 (1996)
22. H. Ota, K. Sakai, R. Aoki, N. Ikemiya, S. Hara: Surf. Sci. **357–358**, 150 (1996)
23. N. Chandrasekhar, V. Agrawal, V.S. Achutharaman, A.M. Goldman: Physica C **205**, 161 (1993)
24. R. Souda, T. Aizawa, Y. Ishizawa, C. Oshima: J. Vac. Sci. Technol. A **8**, 3218 (1990)
25. R.V. Smilgys, S.W. Robey, C.K. Chiang, T.J. Hsieh: J. Vac. Sci. Technol. A **11**, 1361 (1993)
26. T. Minamikawa, T. Suzuki, Y. Yonezawa, K. Segawa, A. Morimoto, T. Shimizu: Jpn. J. Appl. Phys. **34**, 4038 (1995)
27. F. Ahmed, K. Sakai, H. Ota, R. Aoki, N. Ikemiya, S. Hara: J. Low-Temp. Phys. **105**, 1343 (1996)
28. H.-F. Cheng, C.-H. Lin, H.-Y. Lin, J.-T. Lo, T.-F. Tseng, K.-S. Liu, I.-N. Lin: Physica C **230**, 267 (1994)
29. E.J. Tarsa, E.A. Hachfeld, F.T. Quinlan, J.S. Speck: Appl. Phys. Lett. **68**, 490 (1996)
30. H.U. Krebs, Ch. Krauns, X.-G. Yang, U. Geyer: Appl. Phys. Lett. **59**, 2180 (1991)
31. I.D. Raistrick, M. Hawley, J.G. Beery, F.H. Garzon, R.J. Houlton: Appl. Phys. Lett. **59**, 3177 (1991)
32. H.P. Lang, H. Haefke, G. Leemann, H.-J. Güntherodt: Physica C **194**, 81 (1992)
33. D.G. Schlom, D. Anselmetti, J.G. Bednorz, R.F. Broom, A. Catana, T. Frey, Ch. Gerber, H.-J. Güntherodt, H.P. Lang, J. Mannhart: Z. Phys. B: Condens. Matter **86**, 163 (1992)
34. X.-Y. Zhang, D.H. Lownds, S. Zhu, J.D. Budai, R.J. Warmack: Phys. Rev. B **45**, 7584 (1992)
35. A. Catana, J.G. Bednorz, Ch. Gerber, J. Mannhart, D.G. Schiom: Appl. Phys. Lett. **63**, 553 (1993)